

Magneto-electrodynamics at high frequencies in the antiferromagnetic and superconducting states of $\text{DyNi}_2\text{B}_2\text{C}$

Durga P. Choudhury^{1,2}, H. Srikanth¹ and S. Sridhar¹

¹*Physics Department, Northeastern University, Boston, MA 02115*

²*Rome Laboratory, Hanscom Air Force Base, Bedford, MA 01730*

P. C. Canfield

Ames Laboratory, Department of Physics and Astronomy, Iowa State University, IA 50011

(October 28, 2018)

We report the observation of novel behaviour in the radio frequency (*rf*) and microwave response of $\text{DyNi}_2\text{B}_2\text{C}$ over a wide range of temperature (T) and magnetic field (H) in the antiferromagnetic (AFM) and superconducting (SC) states. At microwave frequencies of 10 GHz, the T dependence of the surface impedance $Z_s = R_s + iX_s$ was measured which yields the T dependence of the complex conductivity $\sigma_1 - i\sigma_2$ in the SC and AFM states. At radio frequencies (4 MHz), the H and T dependence of the penetration depth $\lambda(T, H)$ were measured.

The establishment of antiferromagnetic order at $T_N = 10.3\text{ K}$ results in a marked decrease in the scattering of charge carriers, leading to sharp decreases in R_s and X_s . However, R_s and X_s differ from each other in the AFM state. We show that the results are consistent with conductivity relaxation whence the scattering rate becomes comparable to the microwave frequency.

The *rf* measurements yield a rich dependence of the scattering on the magnetic field near and below T_N . Anomalous decrease of scattering at moderate applied fields is observed at temperatures near and above T_N , and arises due to a crossover from a negative magnetoresistance state, possibly associated with a loss of spin disorder scattering at low fields, to a positive magnetoresistance state associated with the metallic nature. The normal state magnetoresistance is positive at all temperatures for $\mu_0 H > 2T$ and at all fields for $T > 15\text{ K}$. Several characteristic field and temperature scales associated with metamagnetic transitions ($H_{M1}(T)$, $H_{M2}(T)$) and onset of spin disorder $H_D(T)$, in addition to T_c , T_N and $H_{c2}(T)$ are observed in the *rf* measurements.

74.25.Ha, 74.25.Nf, 74.72.Ny, 75.20.Hr, 75.40.Gb, 75.50.Ee, 75.90.+w

I. INTRODUCTION

The discovery of superconductivity in the quaternary borocarbides [1,2] has led to a new family of materials with intriguing properties [3,4]. These are the only known intermetallic superconductors containing an appreciable amount of Nickel that have transition temperatures in excess of 10 K. Stoichiometric single phase compounds with the general composition of $R\text{Ni}_2\text{B}_2\text{C}$, where R is a rare earth element, Yttrium or Lutetium have been synthesized [5] and extensively investigated. Most members of this family that exhibit superconductivity also have coexisting antiferromagnetic order, notable exceptions being $\text{YNi}_2\text{B}_2\text{C}$ and $\text{LuNi}_2\text{B}_2\text{C}$ [6]. This system therefore is very useful in studying the interplay between magnetism and superconductivity. The order in temperature in which these two transitions occur as well as the values of the relevant temperature scales associated (T_N for antiferromagnetic transition and T_c for superconducting transition) vary significantly. Although the monotonic decrease in superconducting transition temperature with increasing de Gennes factor of the rare earth is usually attributed to the pair breaking effects of the moments [7], the magnetism in these materials is much

more complex and defies a simple explanation. For one thing, it turns out that the presence of Nickel, hitherto thought to be grossly detrimental to superconductivity because of its pair breaking effects, is relatively benign in these materials and does not contribute significantly to its magnetic properties [8]. Most of the pair breaking comes from the rare earth moments in these systems where they are present.

Recently, superconductivity ($T_c = 6.2\text{ K}$) was reported in $\text{DyNi}_2\text{B}_2\text{C}$, below an antiferromagnetic transition at $T_N = 10.3\text{ K}$ [7,9]. Thus this material is one of a select few materials where superconductivity appears in the presence of long-range magnetic order, some others being systems like $\text{Ho}(\text{Ir}_x\text{Rh}_{1-x})_4\text{B}_4$ [10], $\text{Tb}_2\text{Mo}_3\text{Si}_4$ [11] and some of the heavy fermion superconductors.

Metallic or superconducting antiferromagnets afford the possibility to study the influence of local moments on electronic properties. In the metallic state, interesting effects are expected on the transport properties such as the conductivity. In the superconducting state, magnetism can lead to novel effects on the superconducting order parameter. This is because of the presence of low energy and magnetic field scales in the system, such as spin-flop field scales arising from the magnetic state, and

vortex-related fields due to superconductivity.

High frequency measurements such as those of the surface impedance $Z_s = R_s + iX_s$ yield unique information often not available with other techniques, particularly those at dc or low frequencies such as dc resistivity or ac susceptibility. In the metallic state, information regarding the dynamics of electrons and electronic moments can be obtained. In the superconducting state, the order parameter can be probed in terms of the penetration depth. Because of finite dissipation at high frequencies, one can simultaneously probe the quasiparticle effects too.

In this paper we report our results on measurements of radio frequency (~ 4 MHz) skin depth and microwave (~ 10 GHz) surface impedance on high quality single crystals of this material. Several novel features are reported. A marked decrease in the scattering of charge carriers is observed upon establishment of antiferromagnetic order at $T_N = 10.3$ K. R_s and X_s differ from each other in the antiferromagnetic state, which we show arises from conductivity relaxation. Anomalous decrease of scattering at moderate applied fields is observed at temperatures near and above T_N , and is proposed to arise from changes in spin disorder scattering. Several characteristic field and temperature scales associated with metamagnetic transitions ($H_{M1}(T)$, $H_{M2}(T)$) and a crossover field scale $H_D(T)$, in addition to T_c , T_N and $H_{c2}(T)$ are observed in the *rf* measurements. The behaviour of the complex conductivity in the SC state and the AFM state are obtained as functions of temperature.

II. EXPERIMENTAL DETAILS

A. RF Setup

The *rf* measurements were carried out in a tunnel diode driven tank oscillator self-resonant typically at 4 MHz. The sample is placed in an inductive coil which is part of the L-C tank with the *rf* field H_{rf} , the dc field H_{dc} and the \hat{c} axis oriented such that $H_{rf} \perp H_{dc} \perp \hat{c}$. The inset to Fig.2 shows a picture of this geometry. Magnetic fields upto 70 kOe were applied using a superconducting magnet. This experimental technique has been extensively used to study high and low T_c superconductors both in the Meissner and mixed states [12–14]. If either the skin depth δ or the superconducting penetration depth λ changes as functions of T or H , these changes can be measured as changes Δf in resonant frequency using $\Delta(\delta \text{ or } \lambda) = -G \Delta f$, where G is a geometric factor. The oscillator is ultra-stable, (approximately 1 Hz in 4 MHz), and this leads to very high sensitivity, with typical resolutions of a few Å. Earlier experiments in cuprate superconductors have led to a wide variety of information regarding superconducting parameters such as the lower critical field H_{c1} and pinning forces κ_P [12] and

have also been recently used to study borocarbide superconductors where they have revealed new features in the H - T phase diagram [13,14]. The primary advantage of our technique is the ability to probe both the resistivity in the normal state and superfluid density in the superconducting state which is not possible with conventional techniques such as DC resistivity or AC susceptibility. An interesting example of the versatility and sensitivity of the setup was recently demonstrated when we could resolve an *area preserving* hexagonal to square transition of the flux line lattice in $\text{ErNi}_2\text{B}_2\text{C}$ [15], another member of the borocarbide family, which was not visible in magnetic susceptibility measurements.

The sample was mounted on a sapphire rod with a groove machined on it. Sapphire is a good thermal conductor but a poor electrical conductor; thus while the sample is thermally well anchored to its environment, the contribution of the sample holder to the frequency shift is minimal. The coil was mounted on the sapphire and was attached to a sheet of alumina with GE varnish. The alumina sheet carried an electric heater for fine tuning of the sample temperature. Data acquisition was done by a computer using a GPIB interface.

B. Microwave Setup

The microwave measurements were carried out in a superconducting Niobium cavity using the “cold cavity-hot finger” technique [16]. The cavity is immersed in a bath of liquid Helium, and the sample is mounted on a piece of sapphire inside the cavity. The sapphire has a heater mounted on it so that the temperature of the sample can be varied from below 4 K to above 200 K while the cavity is maintained at a fixed temperature of 4.2 K, as is necessary for it to remain superconducting. The perturbation of the cavity due to the change in the superconducting properties of the sample is reflected as a change of resonance frequency f and bandwidth δf of the cavity. This is related to the change in the complex surface impedance ($Z_s = R_s + iX_s$) as $R_s = \Gamma(1/Q_s(T) - 1/Q_0(T))$ and $\Delta X_s = 2\pi\mu_0 f_0 \Delta\lambda = (-2\Gamma/f_0)(f_s(T) - f_0(T))$ where Γ is a geometric factor relating to the cavity and the sample dimensions, Q_s and Q_0 are the loaded and unloaded quality factor of the cavity ($Q = f/\delta f$), and f_s and f_0 are the loaded and unloaded resonance frequencies respectively. Our setup allows us to measure the absolute value of R_s but only the relative change in X_s . An absolute value is imposed on X_s by assuming that $X_s = R_s$ at high temperatures ($T \gg T_c, T_N$) where any effect of superconductivity or magnetism would be negligible. The superconducting cavity has very high Q , of the order of 10^7 - 10^8 , making it very sensitive to small changes in the surface resistance ($\sim 10\mu\Omega$) and penetration depth ($\sim 1\text{Å}$). An additional advantage of the superconducting cavity is that it shields out stray magnetic fields from the

sample. This technique has been very successfully used to yield a wealth of information on other members of the borocarbide family [17] as well as many high temperature superconductors [18,19]

C. Crystal Growth

High quality single crystals of the material were prepared using the high temperature flux growth technique [20]. This method consists of furnace heating a mass of stoichiometric polycrystalline material with an equal mass of Ni_2B flux in an inert atmosphere. Single crystals of the material grow into the flux in the shape of platelets. The crystals grown this way have relatively large size, making them particularly useful for measurement of bulk properties. The superiority of these crystals in terms of phase purity, proper stoichiometry and low density of defects have been verified by X-ray diffraction and other methods [7]. Typical size of the crystal used in our experiments is $2 \times 0.8 \times 0.2 \text{ mm}^3$.

III. RESULTS AND DISCUSSION

A. Radio Frequency Measurements

These experiments, carried out for $2 \text{ K} < T < 100 \text{ K}$ and $0 < H < 70 \text{ kOe}$ essentially measure the real part of the complex electromagnetic penetration depth $\tilde{\lambda} = \sqrt{\frac{-i}{\mu\omega\sigma}}$ at radio frequencies. In the normal state, $\sigma = \sigma_n$ is the normal conductivity and is purely real. In this case, $\tilde{\lambda}^{-1} = \delta^{-1}(1 + i)$, where $\delta = \sqrt{\frac{2}{\mu\omega\sigma_n}}$ is the skin depth. In the superconducting state, σ has to be replaced with an effective complex conductivity $\sigma_s = \sigma_1 - i\sigma_2$ whose real and imaginary parts are proportional to the quasi-particle scattering and superfluid density respectively. In the limit $\sigma_2 \gg \sigma_1$, which typically holds for $T < T_c$, $\tilde{\lambda} = \frac{1}{\sqrt{\mu\omega\sigma_2}} = \lambda_L$, the London penetration depth. Notice that the normal state skin depth is a factor of $\sqrt{2}$ bigger than the penetration depth. All the data presented in this paper show penetration depths both in the normal and superconducting states and are denoted by λ .

The temperature dependence of λ shows a clear signature of the onset of the magnetic order at 10.3 K, (see fig.1) which has also been observed by other techniques such as neutron scattering and specific heat measurements by other investigators [21–23]. Onset of the superconducting transition brings about further decrease in magnetic field penetration. Note that measurement of DC resistivity also shows a very similar behaviour [7] which is to be expected because of the proportionality between the square root of resistivity and the skin depth

as mentioned above. Although no details of temperature dependence of penetration depth in the superconducting state is visible in DC measurements because of the very nature of the technique, in our setup this information is clearly seen.

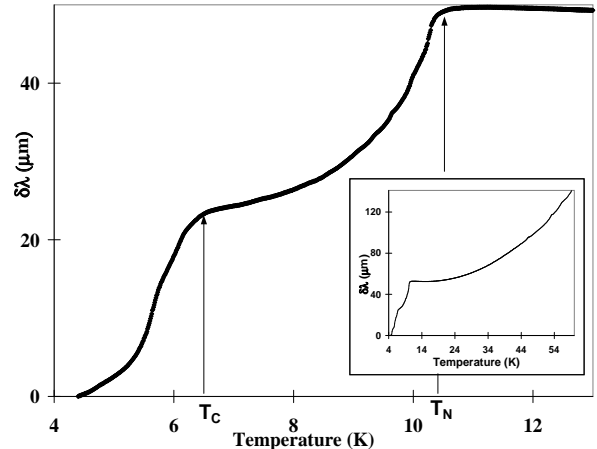


FIG. 1. Electromagnetic screening depth λ against temperature. The onset of superconductivity and the signature of the antiferromagnetic order are quite visible. Notice the similarity with fig.3(a) of ref.7 which is expected because of the proportionality between λ and $\sqrt{\rho}$. Inset: The same data shown over extended temperature range.

The same experiment, done in the presence of a finite DC field, reveals further interesting features. Fig.2 shows typical data taken for $H = 0, 2.5 \text{ kOe}, 5 \text{ kOe}$ and 10 kOe respectively. The inset show the relative orientation of the sample's \hat{c} -axis and the applied dc and rf fields. The direction of the induced rf current is also shown as a reference. Successive curves are shifted along the vertical axis by roughly the same amount to render greater clarity to the figure. Since in this experiment we only measure the *change* in screening length, a constant shift will not affect any of the further discussion. The total change in screening length is shown on the right hand side of each curve. The superconducting transition is still visible but with a depressed T_c in the field-cooled $\lambda(T)$ curve at $H = 2.5 \text{ kOe}$. The application of a magnetic field decreases the sharpness of the change of λ at the antiferromagnetic transition and it appears that at a field greater than the zero temperature H_{c2} , the λ would attain a constant value independent of temperature at very low temperatures. This reflects the residual resistivity of the material. As temperature is increased, a dip appears in the screening length for field scales $\sim 10 \text{ kOe}$. It signals the existence of some mechanism that leads to the reduction in scattering of charge carriers. We shall elaborate on that later in this paper.

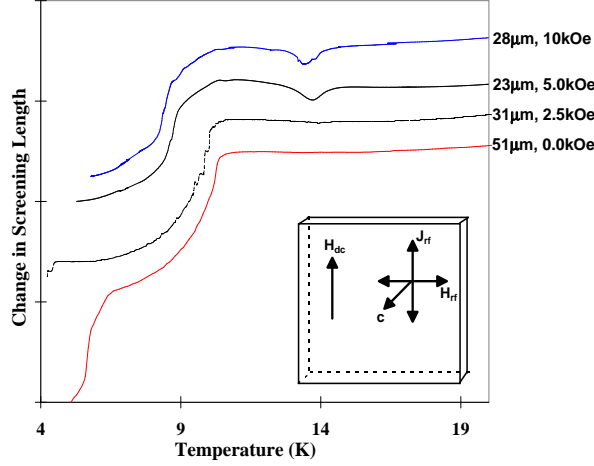


FIG. 2. Radio frequency penetration depth against temperature measured in finite magnetic field. Various data sets have been shifted from each other vertically for clarity of presentation. Inset : Schematic of sample orientation relative to H_{dc} and H_{rf} .

To see these features from another perspective, we did a series of measurements of λ against H at various fixed temperatures and a few typical data sets are shown in Fig.3. The plots for successively increasing temperatures have been displaced from each other along the vertical axis to avoid overlapping, as was done in Fig.2. Several features of the field ramp data, although present in the temperature ramps, are now more obvious. We point them out in the following.

- The magnetic state shows two sharp jumps of the screening length both above and below T_c , originating from metamagnetic transitions in the sample. Such transitions have also been noticed in DC magnetization measurements of $\text{DyNi}_2\text{B}_2\text{C}$ [22,24] as well as in other members of the borocarbide family such as $\text{HoNi}_2\text{B}_2\text{C}$ [25–27]. With the increase of temperature, the magnitude of the jump at field H_{M1} (as defined in Fig.4) decreases and that of the one at H_{M2} increases. As a result of these transitions, the mean free path in the sample decreases rapidly as field is increased from zero to about 10 kOe.
- In the non-superconducting state, regardless of the magnetic order, the resistance goes through a local minimum as the field is swept from zero. The sharpness of this minimum goes down as temperature is increased, and at the highest temperature of 17.7K at which data was taken, this minimum is barely visible. We remark here in passing that the data shown in Fig.2 indicates that the field scale H_D (defined in Fig.4) at which this dip is most pronounced decreases rapidly at $T \sim 13$ K.
- The response of the material at very high field

(> 20 kOe) shows positive magnetoresistance at all temperatures, characteristic of its metallic behaviour. Data is shown only upto 40 kOe in fig.3 for clarity of presentation. Beyond this, λ increases monotonically with field up to 70 kOe, the maximum field at which data was taken.

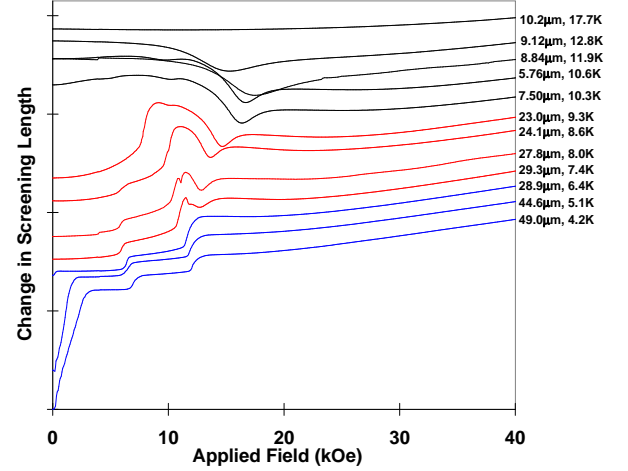


FIG. 3. Screening length against field at various temperatures. Each curve has been displaced along the vertical axis by a fixed amount for better visibility. The total change in screening length $[\lambda(H = 70 \text{ kOe}, T) - \lambda(H = 0, T)]$ is indicated on the right hand side for each curve.

It is obvious from Fig.3 that the screening length is characterized by field scales in addition to the well known scale of H_{c2} . In fig.4 we define the nomenclature for these field scales that we will subsequently be using for discussion throughout this paper. The two field scales corresponding to the metamagnetic transitions are called H_{M1} and H_{M2} respectively and the scale at which skin depth reaches a local minimum for $T > T_c(H = 0)$ is called H_D .

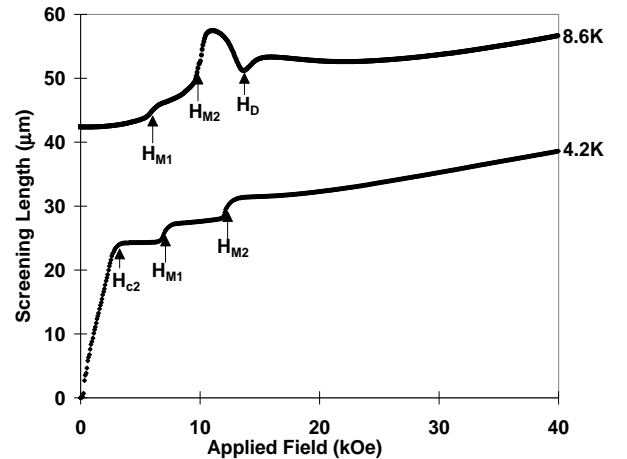


FIG. 4. Characteristic field scales in $\text{DyNi}_2\text{B}_2\text{C}$.

To further analyze these features, we numerically calculated $d\lambda/dH$ for the data shown in Fig.3. Three typical data sets of this kind, one each for the case of $T < T_c$, $T_c < T < T_N$ and $T > T_N$ are shown in fig.5. The characteristic field scales that we discussed above are now much more obvious.

The topic of the interplay between antiferromagnetism and superconductivity has been extensively investigated [28–32]. Many of the “classic” antiferromagnetic superconductors like the Rhodium Boride cluster compounds and $R\text{Mo}_8\text{S}_8$ (R = Rare Earth) are well known to undergo field induced spin-flop transitions in the superconducting state which have been investigated both experimentally [33] and theoretically [34,35]. Such transitions in $\text{DyNi}_2\text{B}_2\text{C}$ occur at H_{M1} and H_{M2} ($> H_{c2}$) after superconductivity has been quenched, either by raising temperature or the applied field.

Above T_N , the magnetoresistance of this material goes through a local minimum with increasing field (Fig.3), the sharpness of which decreases as temperature increases. Although at first inspection this local minimum in magnetoresistance may appear quite novel, we believe that it is associated with a crossover from the negative magnetoresistance associated with the loss of spin disorder scattering from the Dy sublattice as it is aligned along the applied field to the positive magnetoresistance associated with conduction band electrons. These two effects are clearly seen in data taken in the paramagnetic state of $\text{HoNi}_2\text{B}_2\text{C}$ and $\text{LuNi}_2\text{B}_2\text{C}$ [36,37]. Although these two effects do indeed give rise to a local minimum in magnetoresistance in the paramagnetic state they do not give rise to as sharp a local minimum as is seen in the data in fig.3. This enhanced sharpness may be associated with interaction between the local moments since $T \approx T_N$ for these data. Another possible explanation for the local minimum is that it represents an as-of-yet-undetected phase transition line that exists at intermediate fields for a temperature near T_N . Although we currently consider this to be the less likely explanation, the possibility of another phase transition is the subject of ongoing research.

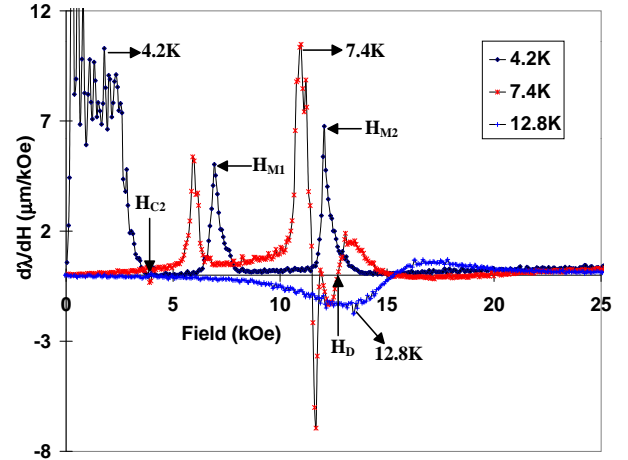


FIG. 5. $d\lambda/dH$ for $\text{DyNi}_2\text{B}_2\text{C}$ at different temperatures.

From the data of Fig.5, we constructed a “phase diagram” for $\text{DyNi}_2\text{B}_2\text{C}$ demarcating the temperature dependence of the various field scales as shown in Fig.6. H_{c2} was defined to be the field at which $d\lambda/dH$ becomes vanishingly small. The values thus obtained are somewhat higher than those obtained from DC measurements [7]. The same criterion was used for determining H_D , the field at which λ goes through a minimum. It is worth mentioning here that H_D most likely a crossover field scale and not does not represent a phase transition as was discussed previously. H_{M1} and H_{M2} , however, represent field scales corresponding to metamagnetic transitions [38] and are chosen so that $d\lambda/dH$ is maximum. The region within the full width at half maximum of each peak is shaded in the diagram demarcating the approximate span of the transition region.

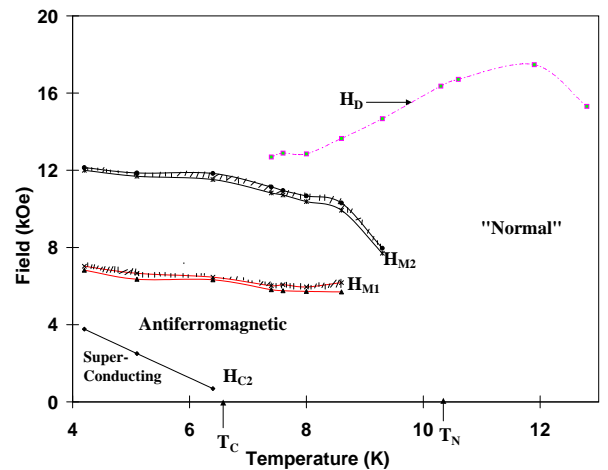


FIG. 6. Temperature dependence of characteristic field scales in $\text{DyNi}_2\text{B}_2\text{C}$. The shaded regions demarcate the regimes of the two metamagnetic transitions. The lines joining the data points are meant to be a guide to the eye.

B. Microwave Measurements

Fig.7 shows the surface impedance at 10 GHz as a function of temperature. For a normal metal, the real and imaginary parts of the surface impedance are equal, as is obvious from elementary electrodynamic considerations [39], and indeed such behaviour is observed in the normal state for all the materials we have studied in our setup so far. However, DyNi₂B₂C is unique in the sense that R_s and X_s (where $Z_s = R_s + iX_s$) differ from each other even in the AFM state below T_N . The quantity with more direct physical relevance is the complex conductivity $\sigma_s = \sigma_1 - i\sigma_2$. This quantity was calculated from our data using the formula $\sigma_1 = \frac{2\mu_0\omega R_s X_s}{(2R_s X_s)^2 + (X_s^2 - R_s^2)^2}$ and $\sigma_2 = \frac{\mu_0\omega (X_s^2 - R_s^2)}{(2R_s X_s)^2 + (X_s^2 - R_s^2)^2}$ and is shown in the inset of Fig.7. The signature of the onset of the magnetic order on σ_s is that the imaginary part is non-zero even in the normal state.

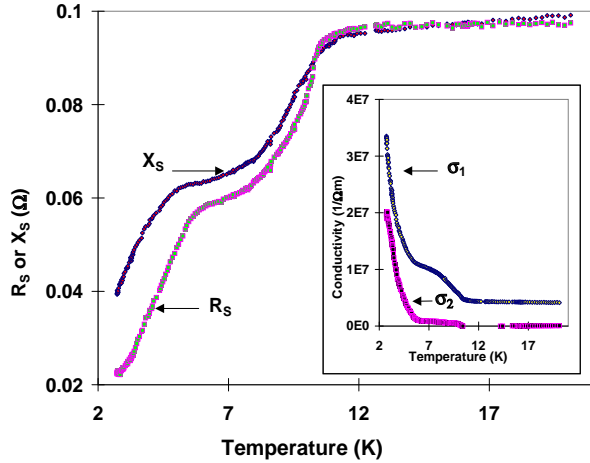


FIG. 7. The real and imaginary parts of the microwave surface impedance of DyNi₂B₂C as a function of temperature. Inset : The real and imaginary parts of the complex conductivity against temperature.

To see this from another perspective, we have plotted the absolute value of the surface impedance, $Z_s(T) = \sqrt{R_s^2 + X_s^2}$, and the phase angle $\theta(T) = \tan^{-1}(X_s/R_s)$ in Fig.8. Although there is an overall similarity of shape of Z_s vs. T between the microwave measurements and the ones measured using the radio frequency technique and the regular 4-probe DC resistivity, the microwave measurements yield additional information associated with conductivity relaxation. For a “conventional” superconductor, the phase angle is expected to change sharply from 45° in the normal state tending towards 90° as $T \rightarrow 0$ below the superconducting transition temperature, and such transitions have indeed been observed by

us for most types of superconductors. Typical data for a single crystal of YNi₂B₂C [17] is shown in the inset of Fig.8 for reference. The phase angle starts to increase relatively sharply at the onset of the antiferromagnetic transition and continues to increase for about 0.5 K below T_N below which it becomes flat again until the superconducting transition sets in. The deviation of θ from 45° in DyNi₂B₂C even before the superconducting transition is a possible consequence of conductivity relaxation and is discussed below. Below the superconducting transition at T_c , θ rises as T is decreased as is expected for a superconductor.

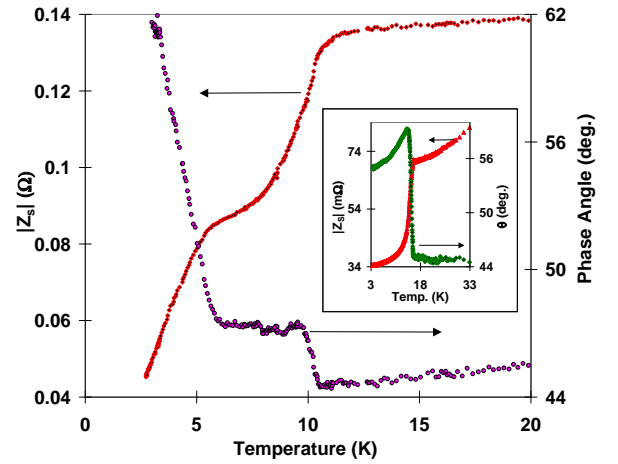


FIG. 8. The magnitude and phase angle of microwave surface impedance of DyNi₂B₂C as a function of temperature. Inset : The same quantities measured on a single crystal of YNi₂B₂C, from ref. 17.

C. Conductivity relaxation in the AFM state

The observed data can be described by a frequency dependent complex conductivity $\sigma(\omega) = \sigma_0/(1+i\omega\tau)$ where σ_0 is the dc conductivity. From $Z_s = \sqrt{\mu_0\omega i/\sigma(\omega)} = (\mu_0\omega/\sigma_0)^{1/2}(i - \omega\tau)^{1/2}$, we obtain the temperature dependence of $\omega\tau(T) = \frac{X_s^2 - R_s^2}{2X_s R_s}$ in the region $T_c < T < 21$ K. The resulting $\omega\tau(T)$ is shown in the bottom panel of Fig.9. Also shown in the same figure on the top is $\rho_0 = 1/\sigma_0 = \frac{2R_s X_s}{\mu_0\omega} = m/ne^2\tau$ where m is the band mass, n is the density of charge carrier, e is the electronic charge and τ is the scattering life time. Finally $\omega_p^2 = \sigma_0/\tau\epsilon_0$ where ω_p is the plasma frequency can also be calculated. For $T < T_N$, $\omega_p \sim 10^{15}$ Hz is comparable to plasma frequencies of other metals.

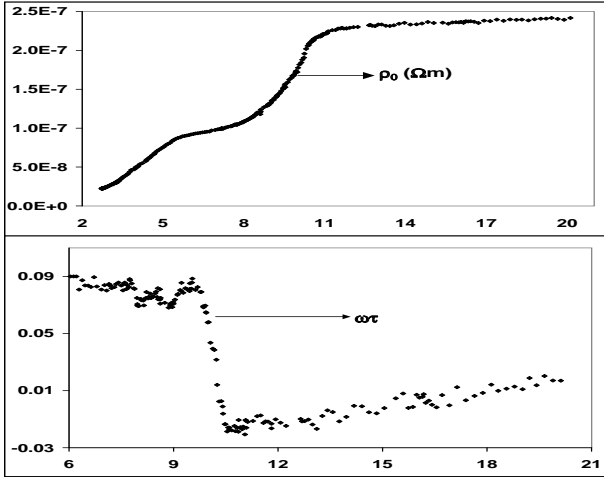


FIG. 9. temperature dependence of some of the material parameters of DyNi₂B₂C. TOP : extracted dc resistivity ρ_0 , BOTTOM: $\omega\tau$ where ω is the measurement frequency and τ is the scattering life time.

For $T > T_N$, $\omega\tau \rightarrow 0$, consistent with $R_s = X_s$ in the normal state. This is the Hagens-Rubens limit of a Drude metal. In the AFM state for $T < T_N$, $\omega\tau$ increases with decreasing T , saturating at a value of around 0.09. This indicates that the scattering rate τ^{-1} approaches a value of 110 GHz. Thus at the measurement frequency of 10 GHz we are pushing into the relaxation regime.

The origin of this conductivity relaxation is related to the development of magnetic order, as is indicated by the temperature dependence of $\omega\tau(T)$. The scattering of conduction electrons by spin waves in the AFM state can give rise to the conductivity relaxation observed here. Conductivity relaxation is also observed in other cases such as spin density wave systems [40] and heavy fermion metals [41].

D. Superconducting state

Since τ is more or less temperature independent for $T_N > T > T_c$ other than the sharp change in the immediate vicinity of T_N , we can plausibly assume that this quantity remains independent of temperature even below T_c in the superconducting state. Since $\omega\tau \sim 0.09$ around T_c , the “effective” conductivity below T_c is assumed to be given by $\sigma_{s,eff} = \sigma_{1,eff} - i\sigma_{2,eff} = (\sigma_1 - i\sigma_2)/(1 + 0.09i)$. Thus we are renormalizing the frequency-dependent conductivity in the superconducting state from the AFM state. The resulting temperature dependence of $\sigma_{1,eff}$ and $\sigma_{2,eff}$ in the superconducting state are shown in Fig.10. Notice that $\sigma_{2,eff} = 0$ for $T > T_c$ which indicates that this quantity is the correct measure of the superfluid density in the system. In the superconducting state, the temperature dependence of $\sigma_{2,eff}$ is anomalously broad and may indicate strong pairbreaking effects [42]. This is the fact that $\sigma_{2,eff}$ continues to rise even for $T < T_c/2$,

atypical of a “conventional” superconductor. The origin of this is the very broad normal to superconducting transition seen in this material which is also observed from dc resistivity measurements [7,43]. This may be related to the strong scattering we have described in earlier in the AFM state. Thus although antiferromagnetism does not inhibit the formation of the superconducting state, it appears to have a strong effect on the electrodynamic properties.

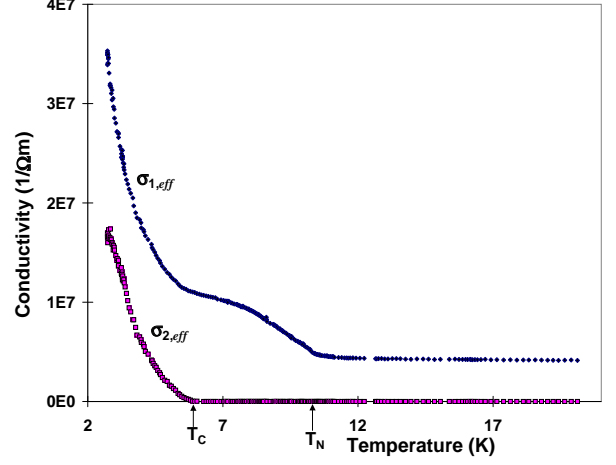


FIG. 10. The “effective” values of σ_1 and σ_2 .

IV. CONCLUSION

In summary, a comprehensive set of measurements of the electrodynamic properties of DyNi₂B₂C in the radio frequency and microwave regimes have been carried out, revealing some very interesting effects of magnetic and superconducting order on transport properties. The presence of magnetic Dy ions strongly affects the transport properties. In the AFM state, establishment of long range magnetic order leads to a strong reduction in scattering. Establishment of antiferromagnetic order gives rise to anomalous increase of electron scattering time which makes the real and imaginary parts of complex microwave surface impedance differ from each other. We have interpreted this behaviour in terms of conductivity relaxation in the AFM state.

Antiferromagnetism also has a distinctive signature on the radio frequency skin depth measurements. The angular dependence of this quantity suggests anisotropic vortex response. Two field induced metamagnetic transitions were observed in the antiferromagnetic state, at all temperatures below T_N . A theoretical framework taking into account the scattering of the conduction electrons from the 2-D sheets of ferromagnetically coupled rare earth moments is likely to be required for a clear understanding of all the observed effects.

While several interesting results have emerged from the present measurements, the results also suggest new avenues to explore in further work and also call for a better theoretical understanding of these novel materials.

V. ACKNOWLEDGMENTS

Stimulating discussions with Balam A. Willemsen, S. Oxx, Benjamin Revcolevschi and T. Jacobs are thankfully acknowledged. This research was supported by the National Science Foundation through grant No. 9623720.

-
- [1] R. Nagarajan *et al.*, Phys. Rev. Lett. **72**, 274 (1994).
 - [2] R. J. Cava *et al.*, Nature **367**, 146 (1994).
 - [3] K. Rathnayaka, D. Naugle, B. Cho, and P. Canfield, Phys. Rev. B **53**, 5688 (1996).
 - [4] Y. D. Wilde *et al.*, Phys. Rev. Lett. **78**, 4273 (1997).
 - [5] R. J. Cava *et al.*, Nature **367**, 252 (1994).
 - [6] H. Eisaki *et al.*, Phys. Rev. B **50**, 647 (1994).
 - [7] B. K. Cho, P. C. Canfield, and D. C. Johnston, Phys. Rev. B **52**, R3844 (1995).
 - [8] M. E. Massalami, S. L. Bud'ko, B. Giordanengo, and E. M. Baggio-Saitovitch, Physica C **244**, 41 (1995).
 - [9] C. V. Tomy, G. Balakrishnan, and D. M. Paul, Physica C **248**, 349 (1995).
 - [10] H. C. Ku, F. Acker, and B. T. Matthias, Phys. Lett. A **76A**, 399 (1980).
 - [11] F. G. Aliev *et al.*, Physica B **194-196**, 171 (1994).
 - [12] D.-H. Wu and S. Sridhar, Phys. Rev. Lett. **65**, 2074 (1990).
 - [13] S. Oxx *et al.*, Physica C **264**, 103 (1996).
 - [14] S. Sridhar *et al.*, Phys. Rev. Lett. **77**, 2145 (1996).
 - [15] M. R. Eskildsen *et al.*, Phys. Rev. Lett. **78**, 1968 (1997).
 - [16] S. Sridhar and W. L. Kennedy, Rev. Sci. Instrum. **59**, 531 (1988).
 - [17] T. Jacobs *et al.*, Phys. Rev. B **52**, R7022 (1995).
 - [18] T. Jacobs *et al.*, Phys. Rev. Lett. **75**, 4516 (1995).
 - [19] H. Srikanth *et al.*, Phys. Rev. B **55**, R14733 (1997).
 - [20] M. Xu *et al.*, Physica C **227**, 321 (1994).
 - [21] P. Dervenagas *et al.*, Physica B **212**, 1 (1995).
 - [22] M. S. Lin *et al.*, Physica C **249**, 403 (1995).
 - [23] J. W. Lynn *et al.*, Physica B **223 & 224**, 66 (1996).
 - [24] P. C. Canfield and S. L. Bud'ko, Journal of Alloys and Compounds, in Press.
 - [25] S. Oxx *et al.*, , to be Published.
 - [26] P. C. Canfield *et al.*, Physica C **230**, 397 (1994).
 - [27] P. C. Canfield *et al.*, Phys. Rev. B **55**, 970 (1997).
 - [28] A. I. Buzdin and L. H. Bulaevskii, Sov. Phys. Usp. **29**, 412 (1986).
 - [29] M. B. Maple, Physica B **215**, 110 (1995).
 - [30] R. Konno, Physica B **206 & 207**, 638 (1995).
 - [31] M. B. Maple and Ø. Fischer, *Superconductivity in Ternary Compounds II : Superconductivity and Magnetism* (Springer-Verlag, New York, 1982), "Topics in Current Physics Vol. 34".
 - [32] M. L. Kulić, A. I. Lichenstein, E. Goreatchkovski, and M. Mehring, Physica C **244**, 185 (1995).
 - [33] H. Iwasaki, M. Ikebe, and Y. Muto, Phys. Rev. B **33**, 4669 (1986).

- [34] A. I. Buzdin, S. S. Krotov, and D. A. Kuptsov, Sol. St. Comm. **75**, 229 (1990).
- [35] O. Wong, H. Umezawa, and J. P. Whitehead, Physica C **158**, 32 (1989).
- [36] I. R. Fisher *et al.*, J. Low. Temp. Phys. **105**, 1623 (1996).
- [37] I. R. Fisher, J. R. Cooper, and P. C. Canfield, Phys. Rev. B , to appear as a brief report.
- [38] Z. Hossain *et al.*, Physica B **223** & **224**, 99 (1996).
- [39] J. D. Jackson, *Classical Electrodynamics*, 2 ed. (Wiley, New York, 1975).
- [40] H. H. S. Javadi *et al.*, Phys. Rev. Lett. **55**, 1216 (1985).
- [41] S. Donovan, A. Schwartz, and G. Grüner, Phys. Rev. Lett. **79**, 1401 (1997).
- [42] B. K. Cho, P. C. Canfield, and D. C. Johnston, Phys. Rev. Lett. **77**, 163 (1996).
- [43] C. V. Tomy *et al.*, Phys. Rev. B **52**, 9186 (1995).